Chem

CellPress

Article

Identifying the Conformational Isomers of Single-Molecule Cyclohexane at Room Temperature

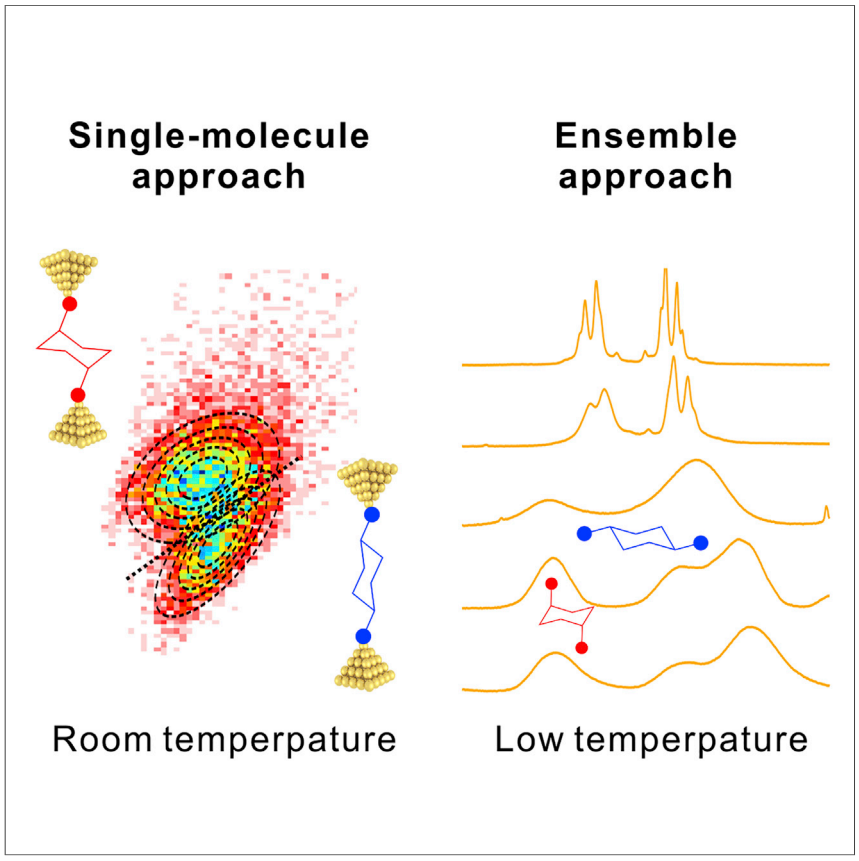

The identification of conformational isomers of the flexible molecule is challenging, owing to the rapid interconversion of isomers. By attaching two electrodes on a flexible molecule, cyclohexane, we accomplish the distinguishment of the two chair isomers of cyclohexane at room temperature using a single-molecule approach. The confinement effect of the attached electrodes not only plays an important role in identifying the chair isomers but also stabilizes the twist-boat intermediate that is showing a negligible distribution in the solution of cyclohexane.

Chun Tang, Yongxiang Tang, Yiling Ye, ..., Jia Shi, Haiping Xia, Wenjing Hong

hpxia@xmu.edu.cn (H.X.)
whong@xmu.edu.cn (W.H.)

HIGHLIGHTS

Identifying conformational isomers of cyclohexane at room temperature

The attached electrodes retard the interconversion of conformational isomers

The confinement effect stabilizes the twist-boat intermediate of cyclohexane

Tang et al., Chem 6, 2770–2781
October 8, 2020
https://doi.org/10.1016/j.chempr.2020.07.024

CellPress

Chem

Article

Identifying the Conformational Isomers of Single-Molecule Cyclohexane at Room Temperature

Chun Tang,[1,2] Yongxiang Tang,[1,2] Yiling Ye,[1] Zhewei Yan,[1] Zhixin Chen,[1] Lijue Chen,[1] Longyi Zhang,[1] Junyang Liu,[1] Jia Shi,[1] Haiping Xia,[1,*] and Wenjing Hong[1,3,*]

SUMMARY

Isomerism reflects the ubiquitous nature that molecules with the same molecular formula show different structures. The interconversion between conformational isomers of flexible molecules is quite fast owing to the low barriers of around 10 kcal mol^{-1}, leading to average signal contributed by all the possible isomers characterized by ensemble methods. On this account, identifying the conformational isomers of flexible molecules at room temperature has a substantial challenge. Here, we develop a single-molecule approach to identify the conformational isomers of cyclohexane at room temperature through the single-molecule electrical characterization. By noise analysis and feature extraction of the conductance of single-molecule junctions, we quantificationally identified two chair isomers of cyclohexane at room temperature, while such identification is only feasible at low temperatures by ensemble characterization. The strategy to apply the single-molecule approach to identify conformational isomers paves the avenue to investigate the isomerization of flexible molecules beyond the ensemble methods.

INTRODUCTION

Conformational isomer is essential to understand the properties of molecules made up of the same atoms but in a different arrangement.[1,2] Among different types of isomers, conformational isomers of flexible molecules are challenging to be isolated and identified. The interconversion between the conformational isomers of flexible molecules is rapid owing to the low isomerization barriers, ensemble methods such as nuclear magnetic resonance (NMR) cannot identify corresponding conformation isomers around room temperature, thus obtaining the ensemble averages contributed by all possible isomers (Figure 1A).[3] Among the flexible molecules, one of the typical flexible molecules is cyclohexane with well-defined conformational isomers, in which two chair conformations are dominated with about 10 kcal mol^{-1} interconversion barrier via a twist-boat intermediate (Figure 1A).[4–6] More importantly, the conformation of cyclohexane has a close relationship to plenty of biomolecules, such as galactose and lactose in pyranose form,[7] showing a six-membered ring similar to cyclohexane (Figure 1B).[8–12] Thus, the room temperature identification of conformational isomers of cyclohexane is crucial to get insight into such flexible molecules, which have a wide range of applications in molecular biology,[13] medicine,[14] and supramolecular chemistry.[15]

The emergence of single-molecule techniques provides the opportunity to probe the properties of individual molecules,[16–22] showing a relative discreteness when

The Bigger Picture

Conformational isomer is a fundamental concept in chemistry, providing the essential view to understand their unique role in molecular biology, medicine, and supramolecular chemistry. However, the interconversion between conformational isomers of the flexible molecule is fast at room temperature, and ensemble methods could only reflect the average contribution from all the conformational isomers, suggesting a significant challenge to distinguish corresponding isomers individually. In this work, we develop a single-molecule method to quantificationally identify the chair isomers of cyclohexane at room temperature beyond ensemble methods. We also demonstrate that the confinement effect of the attaching of electrodes to molecules could help in stabilizing and characterizing the twist-boat intermediate of cyclohexane. Our study provides a promising strategy to study the conformational isomers of flexible molecules and offers an insight into the fields, where flexible molecules play a role.

compared with ensemble approaches (Figures 1A and 1C).[8,23–26] The discreteness provides the potential for applying data analysis method on single-molecule events to extract detailed information.[27–29] Furthermore, the different conformations of the molecular component in single-molecule junctions have distinct charge transport properties,[30–44] which provide the sensitivity to distinguish the difference between similar conformational isomers via charge transport investigations. The single-molecule technique could also introduce a confinement effect,[45,46] which could restrict the degree of freedom of molecular components when the electrodes are attached,[47] providing another opportunity to enhance the distinguishability. Benefiting from the data discreteness, high sensitivity, and confinement effect of the single-molecule technique, the conformational isomers of flexible molecules could be identified even at room temperature beyond thermodynamic averaging in ensemble methods.

In this work, we characterize the charge transport through single-molecule junctions of cyclohexane formed between the two gold electrodes using the scanning tunneling microscopic break junction (STMBJ) technique. We find that the flicker noise of the single-molecule conductance of cyclohexane shows a bimodal distribution, which is associated with the different conformational isomers of cyclohexane. The identification of the conformational isomers of cyclohexane is achieved at room temperature with good distinguishability, showing a ratio consistent with the thermokinetic experiment of NMR characterization below the temperature of 233 K. Moreover, owing to the confinement effect applied to the cyclohexane bridging with two electrodes, we have the opportunity to stabilize and characterize the twist-boat intermediate of cyclohexane.

RESULTS

Molecular Design and Characterization

To form the single-molecule junctions between the two gold electrodes, we introduced anchor groups –SMe or –SAc in cyclohexane **cySMe** and **cySAc** (shown in Figure 2A) with two distinct chair isomers **ee** and **aa**, named by their anchor groups in axial (abbreviated to "**a**") or equatorial (abbreviated to "**e**") positions. The synthesis and characterization of target molecules are shown in Figures S15–S22. The NMR characterization of **cySMe** at room temperature only shows one pattern of signals (Figure 2B, 298 K), contributed by the average of all the conformational isomers that are in rapid interconversion, which is the challenge to identify such kind of conformational isomers at room temperature by NMR and corresponding ensemble methods. When the temperature decreases to 253 K, we first observed a broadening of the NMR signal, suggesting that the interconversion rate between conformational isomers is slowing down and has become comparable to the time scale of the NMR spectrum. Further reducing the temperature from 253 to 233 K leads to a splitting of the broad signals, which are attributed to the two chair isomers of **cySMe** with the ratio between **cySMe-aa** (both anchor group in axial position) and **cySMe-ee** (both anchor group in equatorial position) to be 60: 40. The attribution of NMR signals is shown in Supplemental Information (Figure S13). The ratio indicates that the free energy of **cySMe-aa** is 0.18 kcal mol^{-1} lower than **cySMe-ee**, suggesting a ratio of 54:46 between **cySMe-aa** and **cySMe-ee** at room temperature (298 K). For molecule **cySAc**, we also observe a similar phenomenon (Figure S22), and determine the ratio between **cySAc-aa** and **cySAc-ee** of about 56:44 at room temperature. It is worth noting that the distinguishability for both molecules by NMR is only feasible at the temperature below 233 K (Figures S21 and S22).

[1]State Key Laboratory of Physical Chemistry of Solid Surfaces, Collaborative Innovation Center of Chemistry for Energy Materials (iChEM), College of Chemistry and Chemical Engineering, Xiamen University, Xiamen 361005, China

[2]These authors contributed equally

[3]Lead Contact

*Correspondence: hpxia@xmu.edu.cn (H.X.), whong@xmu.edu.cn (W.H.)

https://doi.org/10.1016/j.chempr.2020.07.024

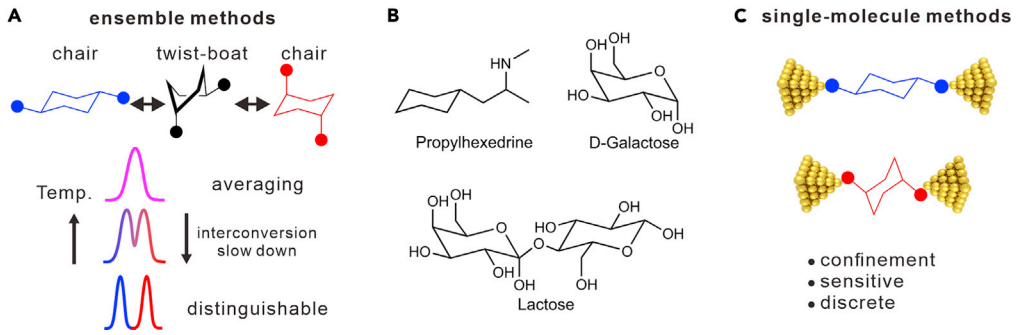

Figure 1. Schematic Illustration of Isomer Identification in Macroscopic and Single-Molecule Scale

(A) Isomerization between two chair isomer cyclohexane is via the twist-boat intermediate. Characterizing cyclohexane by ensemble methods leads to average signal at room temperature, owing to the rapid interconversion of conformational isomers. Reducing temperature slows down such interconversion and makes the conformational isomers distinguishable.

(B) Some examples of the molecules with flexible six-membered rings.

(C) The schematic of the single-molecule technique to characterize the conformational isomers for cyclohexane.

Single-Molecule Conductance Measurement

To characterize the charge transport through single-molecule junctions of **cySMe** and **cySAc**, we carry out the STMBJ experiments in the solution of 0.1 mM target molecules, with 0.1 V bias applied between the gold tip and substrate at room temperature. Through retracting the gold tip connected with the substrate, the plateaus around G_0 firstly form (symbol G_0 is the quantized unit of quantum conductance), which is associated with the formation of gold-gold atomic contact (Figure 2C).[48,49] Further retracting the tip breaks the atomic contacts with another type of plateaus formed in the range from $10^{-5.0}$ to $10^{-6.0}$ G_0, which is the conductance signals of the formed single-molecule junctions. We collected thousands of such conductance traces of **cySMe** (6,370 traces) and **cySAc** (4,031 traces) to construct the one-dimensional (1D) conductance histogram. As shown in Figure 2C, both **cySMe** and **cySAc** have a mono peak centered at $10^{-5.9}$ G_0. The superimposition of conductance traces of **cySMe** leads to the two-dimensional (2D) conductance histogram shown in Figure 2D, which shows about 1.4 nm stretching distance. By adding 0.5 nm gold-gold snap-back distance to the stretching distance,[50] the corrected junction length of **cySMe** is 1.9 nm, which agrees well with the sulfur-to-sulfur distance of **cySMe**. Meanwhile, **cySAc** shows the similar junction lengths to **cySMe** (1.8 nm, Figure 2E), suggesting that the single-molecule junctions of **cySMe** and **cySAc** are formed between two sulfur atoms. The binding strength between the used anchor groups and gold electrodes is reported to be stronger than 0.5 nN,[51–55] which is strong enough to overcome the interconversion barriers between two chair isomers of cyclohexane during the break junction process, leading to the dominant distributions of the stabilized structure during the stretching of junctions.

Variance and Flicker Noise Analysis

Nevertheless, the discreteness of single-molecule characterization provides the opportunity to extract more information than conductance. First, we analyze the variance distributions of break junction traces of the conductance plateaus (Supplemental Experimental Procedures, Section 4). As shown in Figure 3A, we find that the variance distributions of the conductance plateaus of **cySMe** and **cySAc** show bimodal distributions, which are significantly different from a series of control molecules with rigid backbones (Figure S8).

Second, we perform a flicker noise analysis of **cySMe**. The flicker noise of single-molecule junctions contains the information of the electrode-molecule interactions,[27,28,31]

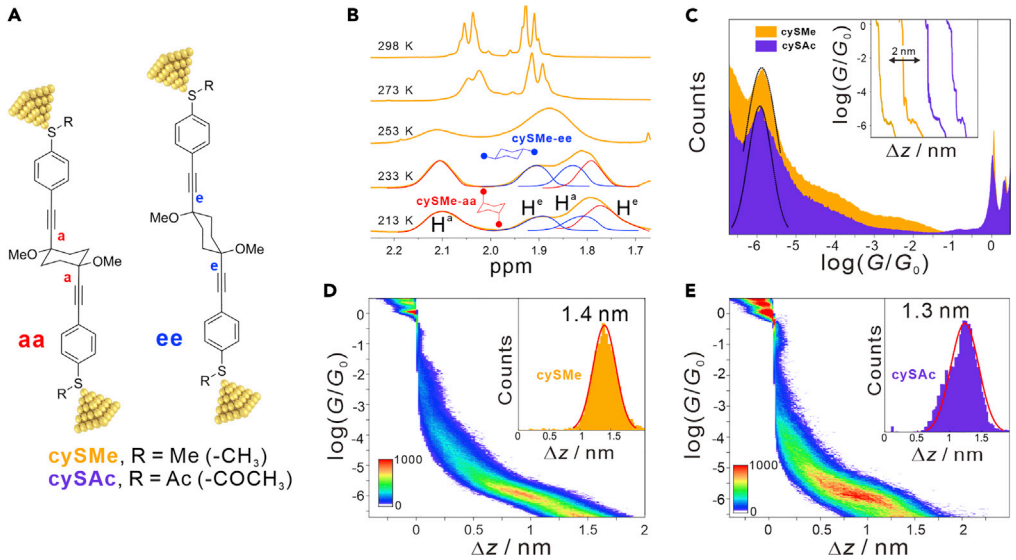

Figure 2. Single-Molecule Conductance Measurement of Cyclohexane

(A) Molecule structures of **cySMe** and **cySAc**, which have two chair conformational isomers, named by "**aa**" and "**ee**," respectively.

(B) Characterizing cyclohexane **cySMe** by NMR at room temperature leads to a dynamic averaging signal. The chair isomers of **cySMe** become distinguishable at low temperatures. The axial hydrogens are labeled as H^a and the equatorial hydrogens are labeled as H^e.

(C) The 1D conductance histograms of **cySMe** and **cySAc** with the typical conductance traces shown in the inset.

(D and E) The 2D conductance histograms of **cySMe** (D) and **cySAc** (E) with the stretching distances shown in the insets.

providing the extra dimension to make such statistical enhancement to distinguish the conformation isomers of cyclohexane. To extract the noise of single-molecule junctions, we suspend the retracting process of the tip for 150 ms once a plateau of the molecular junctions is observed. As shown in Figure 3B, we cut out the data in the region when the tip is suspended. Then, as shown in the inset of Figure 3B, Fourier transformation is applied to the region with the integration from 100 to 1,000 Hz to extract the flicker noise power spectral density (PSD), which is further normalized by the average conductance of the conductance plateau (Supplemental Experimental Procedures, Section 4). The blue and red traces in Figure 3B are two types of typical traces in the experiment of flicker noise analysis, showing a low ($10^{-7.5}$) and high ($10^{-6.1}$) noise PSD, respectively. We could also observe a high-conductance plateau around $10^{-4.5}$ for the trace (red trace in Figure 3B) with high-noise PSD.

We further construct the 2D flicker noise distribution of **cySMe** (7,652 traces). In the 2D flicker noise distribution, each sampling trace is represented by one point in the intensity graph. As shown in Figure 3C, we observe a bimodal distribution in better distinguishability than the variance distributions. We divide the two distributions of flicker noise by the common chord of the boundaries of the two distributions, leading to the ratio between the more dominant one and the other one of ~63:37, which is consistent with the ratio between the two chair isomers of **cySMe** (54:46 between **cySMe-aa** and **cySMe-ee**) at room temperature (Figure 2B). Since the flicker noise of single-molecule junctions highly depends on the electrode-molecule interaction,[27,31] we used another type of anchor group –SAc, to test whether such statistical enhancement facilitated by flicker noise still exist. As shown in Figure 3D, we find that such enhanced distinguishability is also observed in **cySAc**. The flicker noise of **cySAc** also shows a bimodal distribution with a ratio of about 66:34, which is also consistent with the ratio between the two chair isomers of **cySAc** (56: 44 between **cySAc-aa** and **cySAc-ee**, Figure S22). Both **cySMe** and **cySAc** show similar

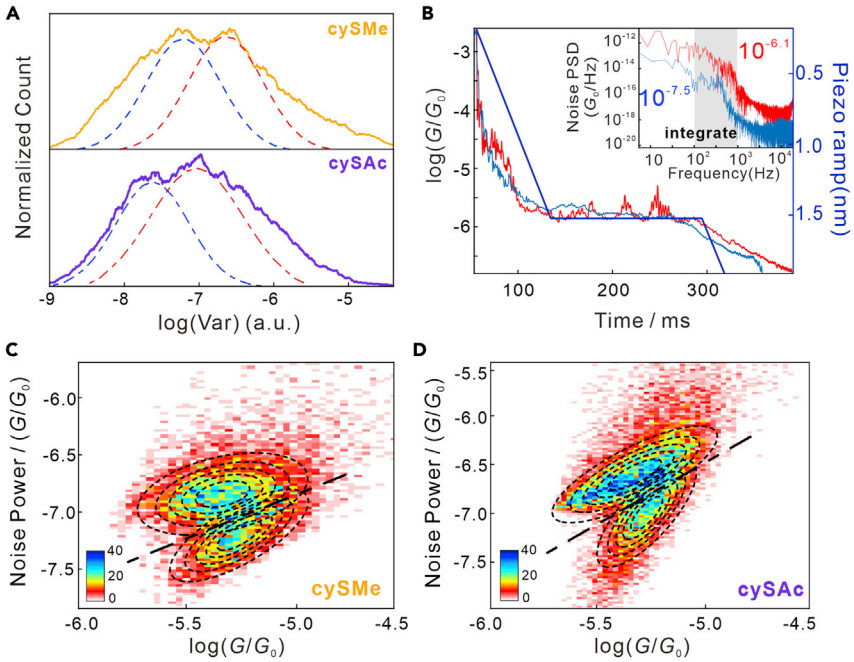

Figure 3. Noise Analysis of the Single-Molecule Junctions

(A) The variance distribution of the conductance plateaus for **cySMe** and **cySAc** during the break junction process.

(B) Typical traces of the flicker noise analysis for the two single traces of **cySMe**, showing strong or weak conductance fluctuation. The data cut out for analysis are in the region when the piezo stops. The corresponding noise power spectrum is shown inset. The flicker noise is achieved by the integration between 100 to 1,000 Hz (shown in the gray region of the inset).

(C and D) The 2D histogram of normalized flicker noise power versus average conductance of **cySMe** (C) and **cySAc** (D); the black cycles are plotted by two-dimensional Gaussian fitting. The black line is the common chord of the fitting curves.

noise distributions, suggesting that the bimodal flicker noise distributions are not from the coupling between electrodes and anchor groups, but mainly contributed by the molecular backbones.

Meanwhile, we find that the traces with different noise distributions (Figure 3) show distinct features. As shown in Figure 3B, the traces (red trace) with a high-conductance plateau around $10^{-4.3}$ G_0, show more substantial fluctuations than the other type of traces (blue trace) without the high-conductance plateaus. We further analyze the flicker noise distribution (Figure 3C) to classify the high-noise and low-noise traces and plot corresponding 2D conductance histogram (Figure S6), showing that the high-noise traces show a distinct plateau around $10^{-4.3}$ G_0. As a control, we perform the same experiment to a series of molecules with a more rigid backbone (Figure S11), only the mono distributions of flicker noise are observed, suggesting that such bimodal distribution of flicker noise for cyclohexane is associated with its conformational isomers. From the above result, we think the dominant flicker noise distribution with high-noise PSD is associated with conformation "**aa**," while the other distribution is associated with conformation "**ee**."

Theoretical Calculation and Data Analysis

We further carry out the theoretical calculation to understand the single-molecule data of cyclohexane isomers. As shown in Figure 4A, the free energy of **cySMe-ee**

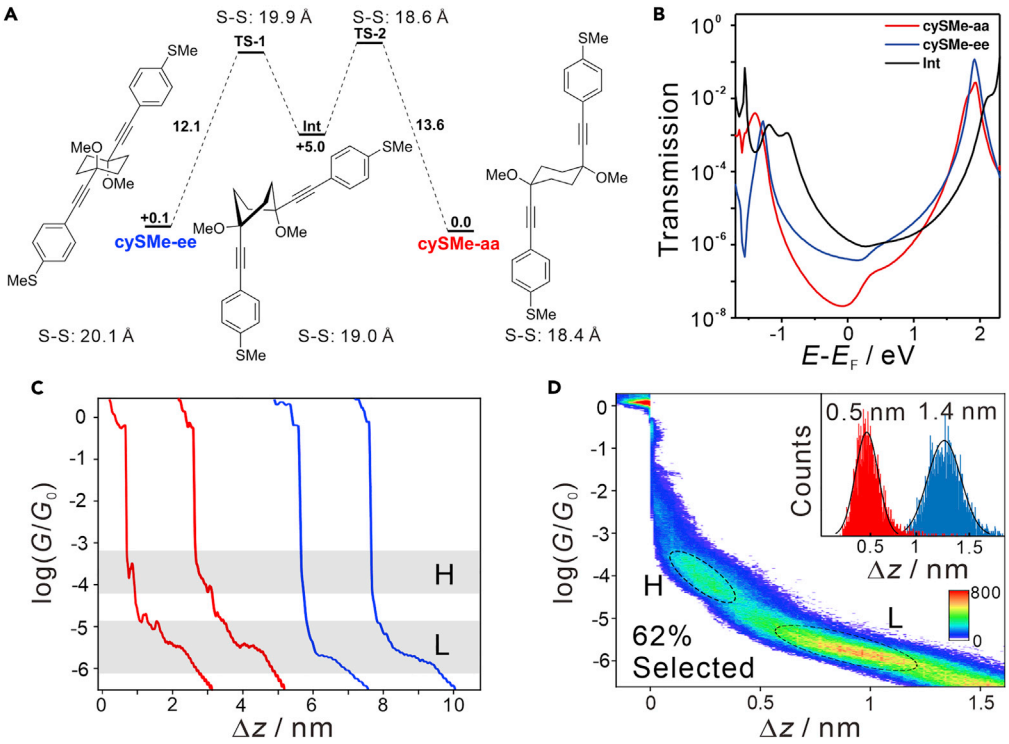

Figure 4. Theoretical Calculation and Conductance Analysis

(A) The calculated interconversion mechanism between **cySMe-ee** and **cySMe-aa** via the intermediate **Int**. The sulfur-to-sulfur distance of each component is shown side by side.

(B) The calculated transmission coefficients of **cySMe-ee**, **cySMe-aa**, and **Int** versus E-E_F.

(C) Two kinds of typical conductance traces of **cySMe**: the traces show two continuous plateaus (red) or only a single plateau (blue). The high and low-conductance regions are labeled by "H" and "L," respectively.

(D) The 2D conductance histogram of **cySMe** of the traces showing two continuous plateaus, with the stretching distances of two plateaus shown in the inset. The high and low conductance are labeled by "H" and "L," respectively, in black cycles.

is 0.1 kcal mol^{-1} higher than that of **cySMe-aa**, which is consistent with the variable temperature NMR (VTNMR) result that the distribution of **cySMe-aa** is more dominated. Also, the interconversion between **cySMe-ee** and **cySMe-aa** is via the intermediate **Int**, a twist-boat geometry, which is about 5.0 kcal mol^{-1} higher than both chair conformations, suggesting that the distribution of **Int** is negligible in comparison with the two chair isomers. The barriers for the interconversion between **cySMe-ee** and **cySMe-aa** are similarly low (12.1 and 13.6 kcal mol^{-1}, respectively), reflecting the rapid interconversion between the two chair isomers. From the sulfur-to-sulfur distances in each component, we find that the theoretical junction lengths are in the following trend: **cySMe-ee** > **Int** > **cySMe-aa**. According to the junction lengths, **cySMe-ee** or **cySMe-aa** would be the stabilized structure during the stretching or compressing of single-molecule junctions, respectively. From the calculated transmission coefficients of the two chair conformations, we find that the transmission probability of **cySMe-aa** is lower than that of **cySMe-ee** in a broad range of energy choices (Figure 4B). Meanwhile, **Int** shows a higher transmission probability than both chair isomers.

From the above results, we expect that the conductance of **cySMe-aa** would be lower than 10^{-7} G_0, which is below the detection limit of our current amplifier. Meanwhile, during the formation of single-molecule junctions of **cySMe**, there are two situations, the **cySMe-ee** or **cySMe-aa** is first captured. If **cySMe-ee** is captured first, since **cySMe-ee**

is fully extended, further stretching of the junction of **cySMe-ee** will not induce the switch of its conformations. On the contrary, if **cySMe-aa** is captured first, the stretching force applied to the shorter junction of **cySMe-aa** will induce the isomerization of **cySMe-aa** to **Int** and finally to **cySMe-ee**. So, it is expected that we could observe a high-conductance state of **Int** only when **cySMe-aa** is captured first. With the aid of the result of noise analysis and calculation, we use a classification method (Supplemental Experimental Procedures, Section 4) to classify the break junction traces of **cySMe** (Figure 2D), and we observe two categories of traces. One of the categories only shows mono conductance plateaus (Figure 4C, blue traces), while the other categories show two continuous conductance plateaus (Figure 4C, red traces), which are located around $10^{-4.3}$ G_0 and $10^{-5.9}$ G_0, respectively. We also perform correlation analysis on **cySMe** and find a positive correlation between the regions of the two conductance plateaus located between [−4.0,−4.5] and [−5.5,−6.0] log(G/G_0), suggesting that the high- and low-conductance plateaus appear simultaneously during the stretching process (Figure S7).[56] The same analysis is also performed on **cySAc**, showing a similar feature with such two categories of traces (Figure S1).

As a comparison, we study a series of molecules with flexible and rigid backbones by STMBJ. We find that flexible molecules are more likely to show multi-conductance plateaus than the rigid molecules (Figure S2), suggesting that the occurrence of such multi-conductance plateaus of **cySMe** or **cySAc** is associated with its corresponding flexibility of backbones. It is worth noting that the pyridine anchor would show a bimodal interaction with gold electrodes,[57,58] so that the use of pyridine anchor in rigid molecules would also show a multi-plateaus feature. Nevertheless, the multi-plateau analysis in the molecules with sulfur anchors shows good consistency with their flexibility of backbones (Figure S2). We think the high-conductance plateaus of **cySMe** around $10^{-4.3}$ G_0 is the signal of the twist-boat intermediate **Int**, which transforms to **cySMe-ee** when the stretching distance is longer than 0.5 nm (Figure 4D, inset). Based on previous studies, a 0.5 nm calibration displacement should be added to the stretching distance, due to the snap back of breaking gold-gold atomic contact.[48,50] So that the actual displacements in Figure 4D should be 1.0 and 1.9 nm for the high- and low-conductance states, respectively. The percentage of those traces showing two conductance plateaus in **cySMe** is 62%, which is associated with the ratio between **cySMe-aa** and **cySMe-ee** by the NMR characterization at low temperature (Figure 2B). We also find that the ratio of the traces of **cySMe** showing two conductance plateaus goes up to 67% in a polar solvent (Figure S24). Since the twist-boat intermediate is unstable in comparison with the two chair isomers of cyclohexane, the distribution of twist-boat intermediate is negligible in solution. Only the chair isomers could be captured first between the two electrodes. When the electrodes first capture the single-molecule junction of **cySMe-aa** in a non-extended form,[59] **cySMe-aa** will show a lower conductance than the through-space tunneling. Further stretching would transform **cySMe-aa** into **Int** with the high-conductance plateaus around $10^{-4.3}$ G_0. Thus, the presence of the high-conductance plateaus could be taken as the event of capturing the single-molecule junctions of **cySMe-aa**. Owing to the involvement of twist-boat intermediate during the stretching of the single-molecule junctions of **cySMe-aa**, the flicker noise of **cySMe-aa** is distinct to **cySMe-ee** (Figure 3C). If the electrodes first capture **cySMe-ee**, since **cySMe-ee** is the stabilized structure during stretching, the conformation of **cySMe-ee** would not be changed by the stretching force.

Single-Molecule Junction in the Close Process

To further study the effect of mechanical force on the single-molecule junction of cyclohexane, we analyze conductance traces when the gold tip is retracting (open process) or

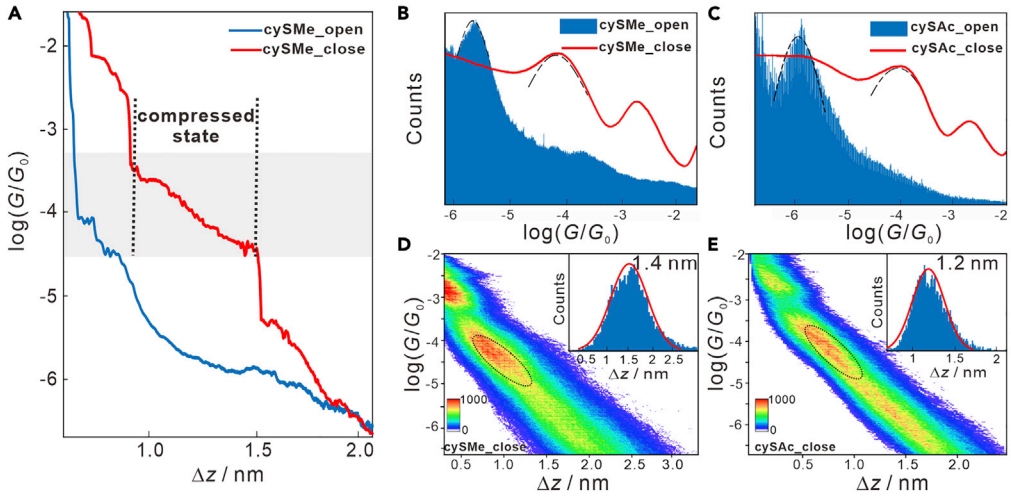

Figure 5. 1D Conductance Histogram of Cyclohexane and Control Molecule Compared with Open and Close Process

(A) The typical traces of the open and close process of **cySMe**. The gray square labels the region.

(B and C) The comparison of the 1D conductance histogram between the open and close process for **cySMe** (B) and **cySAc** (C).

(D and E) The 2D conductance histogram of the close process for **cySMe** (D) and **cySAc** (E) with the stretching distances shown in the insets.

approaching (close process) to the gold substrate. As shown in Figure 5A, we show two typical conductance traces of **cySMe** during the open and close processes. During the open process, the conductance trace shows a conductance plateau around $10^{-6.0}$ G_0, which is different from the close process, showing a conductance plateau around $10^{-4.0}$ G_0. We plot the 1D conductance histograms of **cySMe** during the close process with 6,370 traces. As shown in the red line of Figure 5B, we observe two conductance peaks, located at $10^{-4.3}$ G_0 and $10^{-2.5}$ G_0, respectively. From the control experiment in the blank solvent (1,2,4-trichlorobenzene), the conductance peak at $10^{-2.5}$ G_0 is the signal of the solvent molecule (Figure S4). The conductance peak at $10^{-4.3}$ G_0 is associated with the conductance platitudes of **cySMe** in the close process, showing a significantly high conductance than that during the open process. For **cySAc**, we also observe a significant conductance difference of about $10^{1.8}$ times between the open and close process. As shown in Figures 5D and 5E, the 2D conductance histograms of the close process show that the lengths of the conductance plateaus around $10^{-4.3}$ G_0 are about 1.4 nm, which are close to the lengths of single molecules.

As a comparison, we study the conductance traces for the reference molecules with more rigid backbones, only less than $10^{0.6}$ times difference of conductance is observed between the open and close process (Figures S3B–S3I), showing a similar phenomenon to the reported result.[60] In contrast, flexible molecules show more than ten times the difference of conductance between the open and close process (Figures S3J and S3K). From the above result, we think the chair isomers of cyclohexane are transformed into the twist-boat intermediate when the molecular junctions are compressed, suggesting that the twist-boat intermediate would be the stabilized structure during the compressing of single-molecule junctions. As we discussed above, although the junction length of **cySMe-aa** is shorter than **Int**, the twisted orientation between the two anchor groups in the twist-boat intermediate would be more tolerant of the compressing force. We also perform a reference calculation which also shows the tendency that **Int** would be more tolerant of compressing force (Figure S12). Although the twist-boat conformation is an unstable intermediate of cyclohexane, the confinement effect from electrodes on the molecular component provides the opportunity to stabilize such intermediate.

DISCUSSION

In summary, we develop a single-molecule approach to identify the conformational isomers of cyclohexane at room temperature, while before such identification by NMR is only feasible at the temperature below 233 K. From the characterization of single-molecule conductance combined with noise analysis, we achieve the quantitative identification and enhanced distinguishability between very similar chair isomers of cyclohexane with below 0.2 kcal mol^{-1} difference at room temperature. More importantly, we find that the unstable twist-boat intermediate of cyclohexane could be stabilized by the confinement effect when the two electrodes are bridged by cyclohexane. We demonstrate the potential of analyzing single-molecule events to enhance the distinguishability of similar isomers, which offers the opportunity to investigate the isomerization of flexible molecules beyond the ensemble methods. The enhanced distinguishability of isomers is achieved by the confinement effect of electrodes. Thus, if there is a pair of isomers showing distinct geometries, especially showing distinct lengths, the confinement effect of the attached electrodes would play a role in retarding the isomerization rate. For those isomers that cannot be distinguished by conventional ensemble methods because of the rapid isomerization rate, the retarded isomerization rate by such confinement effect would make it possible to distinguish individual isomers from the single-molecule level.

EXPERIMENTAL PROCEDURES

Resource Availability

Lead Contact

Further information and requests for resources and reagents should be directed to and will be fulfilled by the Lead Contact, Wenjing Hong (whong@xmu.edu.cn).

Materials Availability

The target molecules can be produced following the procedures in the section of the synthesis and characterization in Supplemental Information.

Data and Code Availability

Supplemental Information provides the experimental setup and procedure for STMBJ experiments, the characterization of target molecules, and the algorithms used for the data analysis. Data analysis based on conductance traces, including the construction of 1D histograms and 2D conductance histograms, were conducted by MATLAB programs. The codes generated during this study are available at Github: https://github.com/YXTANGXMU/Single-molecule.

Conductance Measurements

The STMBJ measurements were performed according to previous results.[16,61] The gold tip is made by flame cleaning of 0.25 mm gold wires. We placed about 5 μL of 0.1 mM analyte solutions in 1,2,4-trichlorobenzene (Sigma-Aldrich or Alfa Aesar, 99% purity) on a clean gold-on-mica to perform the STMBJ measurement.

Variance Analysis

According to the previous result,[28] we selected the data ranged between ± 0.5 log(*G*/G0) of the conductance peak (*G*) to analyze the variance fluctuation. We choose the traces with long conductance plateaus (above 0.5 times of the average plateau length). Next, we normalized the traces to eliminate the dimension and strengthen the features of fluctuation. We get the smoothed data by averaging between 20 and 50 neighboring points (the number of averaging is set as the one-tenth of the average plateau length). The normalized traces are obtained by the difference between the raw data and smoothed data. By calculating the standard deviation of

the normalized traces, we get the variance of traces and further plotted the 1D variance distribution histograms.

Flicker Noise Analysis

Flicker noise analysis is performed according to previous results.[27,31,61] We suspended the retracting process of the tip for 150 ms from collecting about 10,000 of such traces and getting the noise spectrum by fast Fourier transform. The noise power is calculated by the noise spectrum integration from 100 to 1,000 Hz, which is plotted against the average conductance.

Computational Details

The structures of **cySMe-ee**, **cySMe-aa,** and **Int** were optimized on Gaussian 16 software package,[62] which also provides the energy of each component. The transmission functions were calculated by Atomistix Tool Kit (ATK) software package.[63] Further calculation details are shown in Supplemental Information.

SUPPLEMENTAL INFORMATION

Supplemental Information can be found online at https://doi.org/10.1016/j.chempr.2020.07.024.

ACKNOWLEDGMENTS

This work was supported by the National Natural Science Foundation of China (nos, 21722305, 21673195, 21703188, and U1705254), the National Key R&D Program of China (2017YFA0204902), China Postdoctoral Science Foundation (no. 2017M622060), and the Fundamental Research Funds for Xiamen University (20720190002).

AUTHOR CONTRIBUTIONS

W.H. and H.X. originally conceived the concept and designed the experiments. W.H., H.X., C.T., Y.T., S.J., J.L., Z.C., and L.C. prepared the manuscript using feedback from other authors. C.T., Y.T., L.Z., and Y.Y. carried out the single-molecule conductance measurements. Y.T. developed the data analysis method. Synthetic work was carried out by C.T. and Z.Y.; calculations were carried out by C.T. All authors approved the final version of the manuscript.

DECLARATION OF INTERESTS

The authors declare no competing interests.

Received: March 24, 2020
Revised: May 14, 2020
Accepted: July 21, 2020
Published: August 24, 2020

REFERENCES

1. Canfield, P.J., Blake, I.M., Cai, Z.L., Luck, I.J., Krausz, E., Kobayashi, R., Reimers, J.R., and Crossley, M.J. (2018). A new fundamental type of conformational isomerism. Nat. Chem. *10*, 615–624.

2. Testa, B. (2013). Organic stereochemistry. Part 8. Helv. Chim. Acta *96*, 1409–1451.

3. Booth, H. (1964). The average coupling constants of protons on adjacent carbon atoms in mobile cyclohexane systems. Tetrahedron *20*, 2211–2216.

4. March, J. (1992). Advanced Organic Chemistry: Reactions, Mechanisms, and Structure (John Wiley & Sons).

5. Carey, F.A., and Sundberg, R.J. (2007). Advanced Organic Chemistry: Part A: Structure and Mechanisms (Springer Science & Business Media).

6. Jensen, F.R., Noyce, D.S., Sederholm, C.H., and Berlin, A.J. (1960). The energy barrier for the chair-chair interconversion of cyclohexane. J. Am. Chem. Soc. *82*, 1256–1257.

7. Hassel, O., Ottar, B., Roald, B., Linnasalmi, A., and Laukkanen, P. (1947). The structure of molecules containing cyclohexane or pyranose rings. Acta Chem. Scand. *1*, 929–943.

8. Im, J., Biswas, S., Liu, H., Zhao, Y., Sen, S., Biswas, S., Ashcroft, B., Borges, C., Wang, X., Lindsay, S., and Zhang, P. (2016). Electronic single-molecule identification of carbohydrate isomers by recognition tunnelling. Nat. Commun. *7*, 13868.

9. Parodi, A.J. (2000). Protein glucosylation and its role in protein folding. Annu. Rev. Biochem. *69*, 69–93.

10. Ohtsubo, K., and Marth, J.D. (2006). Glycosylation in cellular mechanisms of health and disease. Cell *126*, 855–867.

11. Pinho, S.S., and Reis, C.A. (2015). Glycosylation in cancer: mechanisms and clinical implications. Nat. Rev. Cancer *15*, 540–555.

12. Blaszczyk, S.A., Xiao, G., Wen, P., Hao, H., Wu, J., Wang, B., Carattino, F., Li, Z., Glazier, D.A., McCarty, B.J., et al. (2019). S-adamantyl group directed site-selective acylation: applications in streamlined assembly of oligosaccharides. Angew. Chem. Int. Ed. Engl. *58*, 9542–9546.

13. Lawson, C.J., and Rees, D.A. (1970). An enzyme for the metabolic control of polysaccharide conformation and function. Nature *227*, 392–393.

14. Anderson, R.J., Garza, H.R., Garriott, J.C., and Dimaio, V. (1979). Intravenous prophylhexedrine (Benzedrex®) abuse and sudden death. Am. J. Med. *67*, 15–20.

15. Shan, N., Bond, A.D., and Jones, W. (2003). Supramolecular architectures of cyclohexane-1, 3cis, 5cis-tricarboxylic acid in acid:base complexes. New J. Chem. *27*, 365–371.

16. Xu, B., and Tao, N.J. (2003). Measurement of single-molecule resistance by repeated formation of molecular junctions. Science *301*, 1221–1223.

17. Xiang, D., Wang, X., Jia, C., Lee, T., and Guo, X. (2016). Molecular-scale electronics: From concept to function. Chem. Rev. *116*, 4318–4440.

18. Guldi, D.M., Nishihara, H., and Venkataraman, L. (2015). Molecular wires. Chem. Soc. Rev. *44*, 842–844.

19. Reichert, J., Ochs, R., Beckmann, D., Weber, H.B., Mayor, M., and Löhneysen, H.V. (2002). Driving current through single organic molecules. Phys. Rev. Lett. *88*, 176804.

20. Liu, J., Huang, X., Wang, F., and Hong, W. (2019). Quantum interference effects in charge transport through single-molecule junctions: detection, manipulation, and application. Acc. Chem. Res. *52*, 151–160.

21. Xie, Z., Bâldea, I., and Frisbie, C.D. (2019). Determination of energy-level alignment in molecular tunnel junctions by transport and spectroscopy: self-consistency for the case of oligophenylene thiols and dithiols on Ag, Au, and Pt electrodes. J. Am. Chem. Soc. *141*, 3670–3681.

22. Ho Choi, S.H., Kim, B., and Frisbie, C.D. (2008). Electrical resistance of long conjugated molecular wires. Science *320*, 1482–1486.

23. Huang, S., He, J., Chang, S., Zhang, P., Liang, F., Li, S., Tuchband, M., Fuhrmann, A., Ros, R., and Lindsay, S. (2010). Identifying single bases in a DNA oligomer with electron tunnelling. Nat. Nanotechnol. *5*, 868–873.

24. Zhao, Y., Ashcroft, B., Zhang, P., Liu, H., Sen, S., Song, W., Im, J., Gyarfas, B., Manna, S., Biswas, S., et al. (2014). Single-molecule spectroscopy of amino acids and peptides by recognition tunnelling. Nat. Nanotechnol. *9*, 466–473.

25. Huang, C., Jevric, M., Borges, A., Olsen, S.T., Hamill, J.M., Zheng, J.T., Yang, Y., Rudnev, A., Baghernejad, M., Broekmann, P., et al. (2017). Single-molecule detection of dihydroazulene photo-thermal reaction using break junction technique. Nat. Commun. *8*, 15436.

26. Huang, X., Tang, C., Li, J., Chen, L.-C., Zheng, J., Zhang, P., Le, J., Li, R., Li, X., Liu, J., et al. (2019). Electric field–induced selective catalysis of single-molecule reaction. Sci. Adv. *5*, eaaw3072.

27. Adak, O., Rosenthal, E., Meisner, J., Andrade, E.F., Pasupathy, A.N., Nuckolls, C., Hybertsen, M.S., and Venkataraman, L. (2015). Flicker noise as a probe of electronic interaction at metal-single molecule interfaces. Nano Lett *15*, 4143–4149.

28. Inkpen, M.S., Liu, Z.F., Li, H., Campos, L.M., Neaton, J.B., and Venkataraman, L. (2019). Non-chemisorbed gold–sulfur binding prevails in self-assembled monolayers. Nat. Chem. *11*, 351–358.

29. Herrer, I.L., Ismael, A.K., Milán, D.C., Vezzoli, A., Martín, S., González-Orive, A., Grace, I., Lambert, C., Serrano, J.L., Nichols, R.J., and Cea, P. (2018). Unconventional single-molecule conductance behavior for a new heterocyclic anchoring group: pyrazolyl. J. Phys. Chem. Lett. *9*, 5364–5372.

30. Venkataraman, L., Klare, J.E., Nuckolls, C., Hybertsen, M.S., and Steigerwald, M.L. (2006). Dependence of single-molecule junction conductance on molecular conformation. Nature *442*, 904–907.

31. Garner, M.H., Li, H., Chen, Y., Su, T.A., Shangguan, Z., Paley, D.W., Liu, T., Ng, F., Li, H., Xiao, S., et al. (2018). Comprehensive suppression of single-molecule conductance using destructive σ-interference. Nature *558*, 415–419.

32. Li, H.X., Garner, M.H., Shangguan, Z.C., Zheng, Q.W., Su, T.A., Neupane, M., Li, P.P., Velian, A., Steigerwald, M.L., Xiao, S.X., et al. (2016). Conformations of cyclopentasilane stereoisomers control molecular junction conductance. Chem. Sci. *7*, 5657–5662.

33. Leary, E., Roche, C., Jiang, H.W., Grace, I., González, M.T., Rubio-Bollinger, G., Romero-Muñiz, C., Xiong, Y.Y., Al-Galiby, Q., Noori, M., et al. (2018). Detecting mechanochemical Atropisomerization within an STM break junction. J. Am. Chem. Soc. *140*, 710–718.

34. Gerhard, L., Edelmann, K., Homberg, J., Valášek, M., Bahoosh, S.G., Lukas, M., Pauly, F., Mayor, M., and Wulfhekel, W. (2017). An electrically actuated molecular toggle switch. Nat. Commun. *8*, 14672.

35. Frisenda, R., Janssen, V.A.E.C., Grozema, F.C., van der Zant, H.S.J., and Renaud, N. (2016). Mechanically controlled quantum interference in individual pi-stacked dimers. Nat. Chem. *8*, 1099–1104.

36. Perrin, M.L., Frisenda, R., Koole, M., Seldenthuis, J.S., Gil, J.A.C., Valkenier, H., Hummelen, J.C., Renaud, N., Grozema, F.C., Thijssen, J.M., et al. (2014). Large negative differential conductance in single-molecule break junctions. Nat. Nanotechnol. *9*, 830–834.

37. Carini, M., Ruiz, M.P., Usabiaga, I., Fernández, J.A., Cocinero, E.J., Melle-Franco, M., Diez-Perez, I., and Mateo-Alonso, A. (2017). High conductance values in π-folded molecular junctions. Nat. Commun. *8*, 15195.

38. Zhang, N., Lo, W.Y., Cai, Z., Li, L., and Yu, L. (2017). Molecular rectification tuned by through-space gating effect. Nano Lett *17*, 308–312.

39. Chen, X., Roemer, M., Yuan, L., Du, W., Thompson, D., del Barco, E., and Nijhuis, C.A. (2017). Molecular diodes with rectification ratios exceeding 105 driven by electrostatic interactions. Nat. Nanotechnol. *12*, 797–803.

40. Su, T.A., Li, H., Steigerwald, M.L., Venkataraman, L., and Nuckolls, C. (2015). Stereoelectronic switching in single-molecule junctions. Nat. Chem. *7*, 215–220.

41. Thompson, D., and Nijhuis, C.A. (2016). Even the odd numbers help: failure modes of SAM-based tunnel junctions probed via odd-even effects revealed in synchrotrons and supercomputers. Acc. Chem. Res. *49*, 2061–2069.

42. Kim, Y., Song, H., Strigl, F., Pernau, H.F., Lee, T., and Scheer, E. (2011). Conductance and vibrational states of single-molecule junctions controlled by mechanical stretching and material variation. Phys. Rev. Lett. *106*, 196804.

43. Kim, Y., Song, H., Kim, D., Lee, T., and Jeong, H. (2010). Noise characteristics of charge tunneling via localized states in metal–molecule–metal junctions. ACS Nano *4*, 4426–4430.

44. Song, Y., and Lee, T. (2017). Electronic noise analyses on organic electronic devices. J. Mater. Chem. C *5*, 7123–7141.

45. Abb, S., Tarrat, N., Cortés, J., Andriyevsky, B., Harnau, L., Schön, J.C., Rauschenbach, S., and Kern, K. (2019). Carbohydrate self-assembly at surfaces: STM imaging of sucrose conformation and ordering on Cu(100). Angew. Chem. Int. Ed. Engl. *58*, 8336–8340.

46. Marszalek, P.E., Pang, Y.-P., Li, H., El Yazal, J.E., Oberhauser, A.F., and Fernandez, J.M. (1999). Atomic levers control pyranose ring conformations. Proc. Natl. Acad. Sci. USA *96*, 7894–7898.

47. Reisner, W., Beech, J.P., Larsen, N.B., Flyvbjerg, H., Kristensen, A., and Tegenfeldt, J.O. (2007). Nanoconfinement-enhanced conformational response of single DNA molecules to changes in ionic environment. Phys. Rev. Lett. *99*, 058302.

48. Yanson, A.I., Bollinger, G.R., van den Brom, H.E., Agraït, N., and van Ruitenbeek, J.M. (1998). Formation and manipulation of a metallic wire of single gold atoms. Nature *395*, 783–785.

49. Agraït, N., Yeyati, A.L., and van Ruitenbeek, J.M. (2003). Quantum properties of atomic-sized conductors. Phys. Rep. *377*, 81–279.

50. Hong, W., Manrique, D.Z., Moreno-García, P., Gulcur, M., Mishchenko, A., Lambert, C.J., Bryce, M.R., and Wandlowski, T. (2012). Single molecular conductance of tolanes: experimental and theoretical study on the junction evolution dependent on the anchoring group. J. Am. Chem. Soc. *134*, 2292–2304.

51. Aradhya, S.V., Meisner, J.S., Krikorian, M., Ahn, S., Parameswaran, R., Steigerwald, M.L., Nuckolls, C., and Venkataraman, L. (2012). Dissecting contact mechanics from quantum interference in single-molecule junctions of stilbene derivatives. Nano Lett *12*, 1643–1647.

52. Frei, M., Aradhya, S.V., Hybertsen, M.S., and Venkataraman, L. (2012). Linker dependent bond rupture force measurements in single-molecule junctions. J. Am. Chem. Soc. *134*, 4003–4006.

53. Leary, E., La Rosa, A., González, M.T., Rubio-Bollinger, G., Agraït, N., and Martín, N. (2015). Incorporating single molecules into electrical circuits. The role of the chemical anchoring group. Chem. Soc. Rev. *44*, 920–942.

54. Huang, Z., Chen, F., Bennett, P.A., and Tao, N. (2007). Single molecule junctions formed via Au-thiol contact: stability and breakdown mechanism. J. Am. Chem. Soc. *129*, 13225–13231.

55. Xu, B., Xiao, X., and Tao, N.J. (2003). Measurements of single-molecule electromechanical properties. J. Am. Chem. Soc. *125*, 16164–16165.

56. Makk, P., Tomaszewski, D., Martinek, J., Balogh, Z., Csonka, S., Wawrzyniak, M., Frei, M., Venkataraman, L., and Halbritter, A. (2012). Correlation analysis of atomic and single-molecule junction conductance. ACS Nano *6*, 3411–3423.

57. Quek, S.Y., Kamenetska, M., Steigerwald, M.L., Choi, H.J., Louie, S.G., Hybertsen, M.S., Neaton, J.B., and Venkataraman, L. (2009). Mechanically controlled binary conductance switching of a single-molecule junction. Nat. Nanotechnol. *4*, 230–234.

58. Aradhya, S.V., Frei, M., Hybertsen, M.S., and Venkataraman, L. (2012). Van der Waals interactions at metal/organic interfaces at the single-molecule level. Nat. Mater. *11*, 872–876.

59. Huang, C., Rudnev, A.V., Hong, W., and Wandlowski, T. (2015). Break junction under electrochemical gating: testbed for single-molecule electronics. Chem. Soc. Rev. *44*, 889–901.

60. Liu, J., Zhao, X., Zheng, J., Huang, X., Tang, Y., Wang, F., Li, R., Pi, J., Huang, C., Wang, L., et al. (2019). Transition from tunneling leakage current to molecular tunneling in single-molecule junctions. Chem *5*, 390–401.

61. Tang, C., Chen, L., Zhang, L., Chen, Z., Li, G., Yan, Z., Lin, L., Liu, J., Huang, L., Ye, Y., et al. (2019). Multicenter-bond-based quantum interference in charge transport Through single-molecule carborane junctions. Angew. Chem. Int. Ed. Engl. *58*, 10601–10605.

62. Frisch, M., Trucks, G., Schlegel, H., Scuseria, G., Robb, M., Cheeseman, J., Scalmani, G., Barone, V., Petersson, G., Nakatsuji, H., et al. (2016). Gaussian 16. In Revision A (Wallingford CT: Gaussian, Inc.). https://gaussian.com/.

63. Soler, J.M., Artacho, E., Gale, J.D., Garcia, A., Junquera, J., Ordejon, P., and Sanchez-Portal, D. (2002). The SIESTA method for ab initio order-N materials simulation. J. Phys. Condens. Matter *14*, 2745–2779.